Geomorphology 259 (2016) 30–39

Contents lists available at ScienceDirect

Geomorphology

journal homepage: www.elsevier.com/locate/geomorph

Initial insights into the age and origin of the Kubuqi sand sea of northern China

Xiaoping Yang [a,*], Steven Forman [b], Fangen Hu [a], Deguo Zhang [a], Ziting Liu [c], Hongwei Li [a]

[a] Key Laboratory of Cenozoic Geology and Environment, Institute of Geology and Geophysics, Chinese Academy of Sciences, P.O. Box 9825, Beijing 100029, China
[b] Geoluminescence Dating Research Laboratory, Department of Geology, Baylor University, One Bear Place 97354, Waco, TX 76798, USA
[c] School of Environment and Planning, Liaocheng University, Liaocheng 252000, China

ARTICLE INFO

Article history:
Received 9 September 2015
Received in revised form 2 February 2016
Accepted 3 February 2016
Available online 4 February 2016

Keywords:
Aeolian record
Landform
Surface process
Dune
Climate change
Human activity
Holocene

ABSTRACT

The Kubuqi Desert is the only active sand sea in the semiarid regions of northern China and occurs along the southern margin of the Yellow River. Little is known about the age and origin of this large (17,000 km^2) sand sea with a present annual precipitation of 200-480 mm. Sand drift potentials indicated net capable winds for aeolian transport are from the northwest, though winds are stronger to north beyond the dune field than within the sand sea. Geomorphic and stratigraphic observations indicate that Holocene aeolian sand often drapes over bedrock and river terraces as a palimpsest landscape. Field investigations identified four stratigraphic sections with multiple aeolian sand units and palaeosols, with age control by optically stimulated luminescence (OSL) dating of quartz grains. Palaeosols are weakly developed, mostly accumulative A horizon with organic carbon content <1% and reflect sand sheet deposition possibly in a steppe environment. Although sediments near river channels or former lakes might give old ages, the initial formation and age of the Kubuqi sand sea should be judged from the occurrence of the sandy palimpsest of the landscape that is OSL dated to the Holocene in general. The latest period of aeolian reactivation may be related to human activity associated with grazing and farming from *lost* cities in the Kubuqi Desert during the Han (206 B.C. – A.D. 220) and the Tang (A.D. 608 – 907) Dynasties. Also, variable discharge of the Yellow River with local diversions for irrigation and throughout the catchment resulted in possibly an increased supply of aeolian particles for dune field expansion in the past 2 ka.

1. Introduction

Aeolian sand depositional records are valuable palaeoclimatic proxies in arid and semiarid regions because sedimentary sequences with palaeosols reflect changes in sand supply, availability, and wind speed and direction, which often reflect broader changes in synoptic climatology (Lancaster, 1995; Williams et al., 1998; Tooth, 2008; Williams, 2014a, b). Globally, drylands today occur in diverse topographic, ecologic, and climatic settings (Hövermann, 1985; Busche, 1998; Goudie, 2002; Embabi, 2004; Eitel et al., 2005). Thus reconstruction of aeolian depositional process provides unique insights into broader environmental changes (Thomas, 2011; Yang et al., 2011). Generally speaking, aeolian sand deposition mainly occurs in two kinds of landscapes in the arid and semiarid regions of China: sandy deserts and sandy lands. The terminology sandy deserts are restricted to the sand seas with active dunes, and the sandy lands refer to areas of dunes fixed by vegetation. Sand seas occur in areas where the mean annual precipitation (MAP) is <200 mm, while sandy lands are characterized by a MAP between 200 and 450 mm (e.g., Zhu et al., 1980; Yang et al., 2012). Here the availability of sediment is controlled principally by the vegetation coverage that impedes erosion and sediment transport (Kocurek and Lancaster, 1999). The boundary between sand seas and sandy lands is often associated with the climatic shift between arid and semiarid regions and associated zonal vegetation in northern China (Domrös and Peng, 1988). However, China has one active sand sea, the Kubuqi Desert, in the semiarid zone; and this sand sea (erg) remains an environmental enigma.

The Kubuqi sand sea occurs in a relatively wet environment, but little is known about its age, formation, and associated palaeoenvironments. In contrast to earlier theories of the extreme longevity of the deserts in northern China (e.g., Liu, 1985), recent studies of physical and biochemical proxies in the sediments and optical ages indicate that many dunes in the drylands of eastern Asia were formed first in the late Pleistocene and some even in the Holocene. Large-scale stabilization of the dunes occurred in the eastern part of the desert belt during the middle Holocene (e.g., Yang and Scuderi, 2010; Yang et al., 2013). How the nature of aeolian activity in the Kubuqi Desert would have looked during this period is uncertain. This sand sea may reflect arid climate in China in the recent past (Zhu et al., 1980). However, palaeoclimate interferences based solely on aeolian records may not be definitive because of the complex response of dune systems to changing hydroclimatic factors, as the more recent reinterpretations of dune records reconfirm (Telfer and Hesse, 2013). For example, in Muhs and Holliday's (1995) process-response model of impacts of climate change on fluvial and aeolian activity, changes to the

* Corresponding author.
E-mail address: xpyang@mail.igcas.ac.cn (X. Yang).

http://dx.doi.org/10.1016/j.geomorph.2016.02.004
0169-555X/

fluvial regime and channel characteristics caused by a decrease in precipitation would increase sand supply and aeolian activity. However, other studies suggest that enhanced aeolian activity can arise from the development of landscape features often associated with increased precipitation, such as lakes, and fluvial sediment supply (Williams, 1994; Cohen et al., 2010). In south African deserts, the earlier four phases of aeolian activity during 74.5–61, 48.5–41, 33–31 and 23.5–16 ka correlate not with aridity, as might be predicted, but with increased humidity, windiness, and fluvial sediment supply; increased aridity resulting from higher temperatures and reduced moisture during the period of 8–4 ka, however, trigged widespread dune remobilization (Chase, 2009).

This study presents the geomorphologic context and inferred processes for the Kubuqi sand sea in the semiarid zone of northern China, the initial depositional ages by OSL dating, potential palaeoclimatic associations, and the anthropogenic impacts for dune re-activation.

2. Regional settings

Located on the southern bank of the Yellow River, the Kubuqi sand sea extends ~300 km from west to east, and its width decreases from ~100 km in the west to 20–30 km in the east (Figs. 1 and 2). Ten tributaries (permanent and seasonal rivers) of the Yellow River with headwaters in the northern Ordos Plateau flow through the mid and eastern part of the sand sea northward. Aeolian deposits appear to overlie fluvial terraces of the Yellow River and tributaries. The basement of the Kubuqi sand sea is part of the northern Erdos Plateau that consists largely of Cretaceous and Tertiary mudstone, marlite, shale, and clasolite (Ma, 2002). Under the impact of the East Asian Summer Monsoon, the mean annual precipitation decreases from ca. 480 mm in the east to 200 mm in the western portion of the sand sea. Despite the relatively high precipitation, 80% of the dunes in Kubuqi are active (Zhu et al., 1980). Tall transverse dunes (up to 100 m) are perpendicular to the predominant WWN winds and bury apparently fluvial terraces of the Yellow River's tributaries. Barchan dunes are common with a height of a few meters with intervening thin sand-sheet deposits covering various bedrock landforms.

3. Materials and methods

Field investigation was carried out in the Kubuqi Desert from east to west, and we were able to go deep into the dune belt along the stream channels crossing the desert. Aeolian, fluvial sediments, and palaeosols were recognized based on bedding characteristics, color, texture, and carbonate content. To quantify the particle size characteristics, samples were collected from active and vegetation-stabilized dune ridges (samples 2, 3, 6, and 7; Fig. 2). Granulometry was determined with a RETSCH AS 200 Control Vibratory Size Shaker. The mean grain size (Mz), standard deviation (σ), skewness (S_K) and kurtosis (K_G) were calculated following Folk and Ward (1957).

One natural section [c] and three freshly dug sections (a, b, and d in Fig. 2) were studied in detail to better understand landscape evolution and to infer palaeoenvironments. Sediment samples were taken from the freshly dug walls at 10-cm intervals from section [a], 5-cm intervals from section [b], and 20-cm intervals from section [d], depending on the nature of sedimentary changes. In locations with pronounced changes in sedimentary facies, additional subsamples were collected.

To infer palaeoenvironmental processes, physical and biochemical indicators of environmental conditions were examined. Grain size was measured for active and inactive dunes by dry sieving. The content of calcium carbonate was measured with a volumetric calcimeter (Eijkelkamp Corp., Netherlands) that directly determines the amount of CO_2 after the samples react with HCl in a closed system under

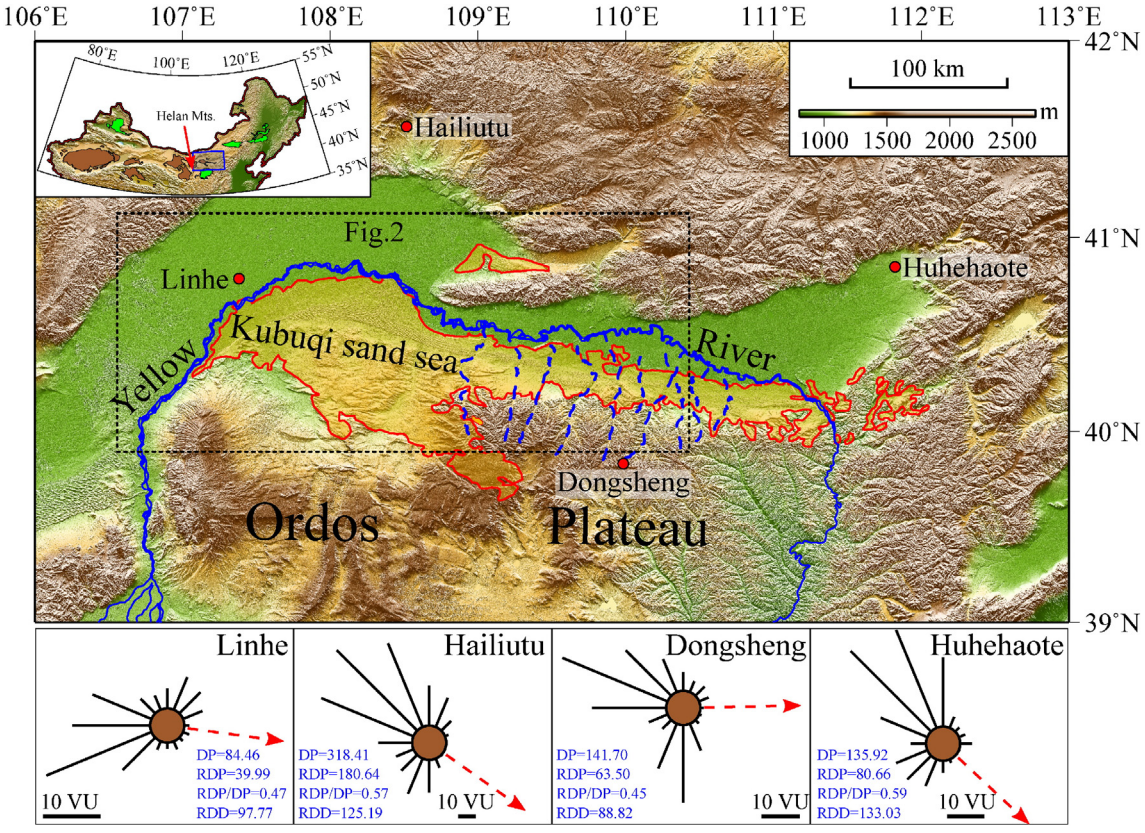

Fig. 1. Overview of the study area. Upper: Location of the Kubuqi Desert (marked in yellow with red contour lines), the main channel being the Yellow River and the dashed lines being the tributaries of the Yellow River flowing from the southern highlands (the Erdos Plateau). The Helan Mountains, stretching N ~ S (106° E), act as a boundary between the arid and semiarid zones. In the inset figure, brown areas are sand seas and green areas mark large sandy lands (Yang et al., 2011). Lower: Wind data of the region, data from the local weather stations. DP, Drift Potential; RDP, Resultant Drift Potential; RDP/DP, wind direction variability and RDD, Resultant Drift Direction (Fryberger and Dean, 1979).

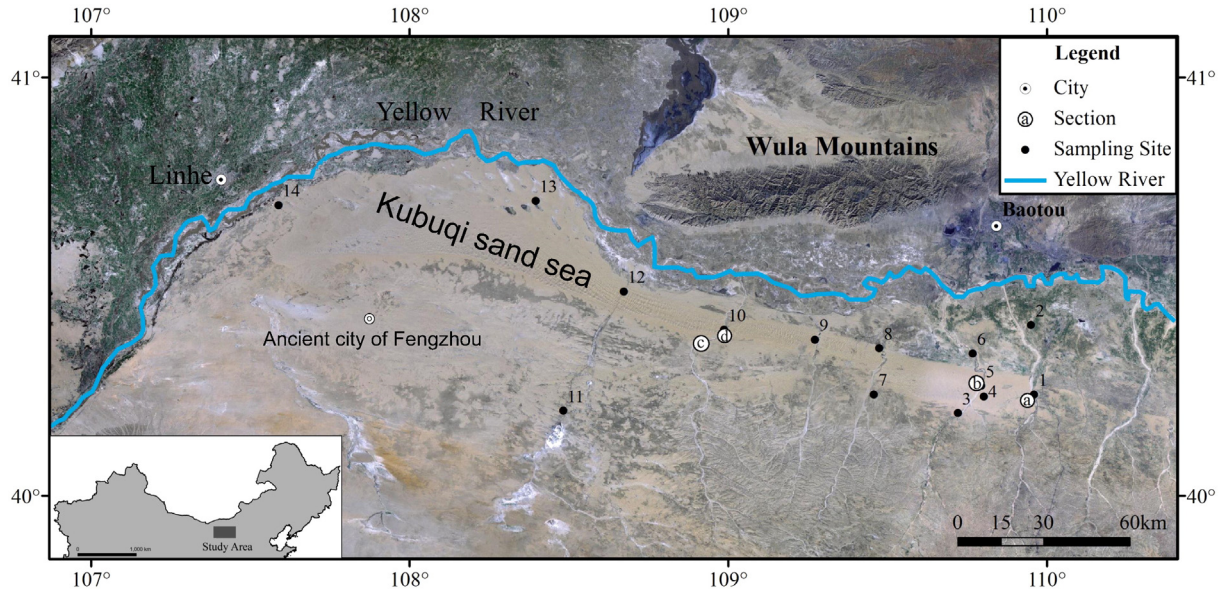

Fig. 2. Sampling sites and locations of sedimentary sections dated by OSL (for geographical coordinates of the sections and sampling sites see Supplementary Table 1).

constant pressure and temperature and in the absence of other gases. The error for the measurement of the calcium carbonate is <±5%. The total carbon (TC, %) and total organic carbon (TOC, %) were examined with an Elementar Rapid CS Cube that employs a highly sensitive cuvette multichannel infrared detector to measure the quantities of CO_2 from the combustion of carbon in the samples. After combustion at 950 °C, the carbon in the samples was fully converted to CO_2, and from that the percentage of total carbon was calculated. The subsamples designated for measuring the TOC were first treated with 18% hydrochloric acid to dissolve inorganic carbon. After the inorganic carbon was removed, the procedure for measuring the TOC with the CS Cube was the same as for measuring the TC, with a relative analytical error < ±1%. Magnetic susceptibility (MS) was measured with a Bartington MS2 susceptibility meter with a calibration accuracy of ±1%. Measurements involved two magnetic fields reading at the frequency of 470 Hz (low field) and 4700 Hz (high field), and the unit of mass-specific MS expressed in m^3kg^{-1} was applied following Dearing (1999). The percentage frequency dependent susceptibility was calculated from these two readings with the value indicating the presence of ultrafine superparamagnetic ferrimagnetic minerals produced by biochemical processes in soil (Dearing, 1999).

The samples were dated in the OSL (optically stimulated luminescence) Dating Research Laboratory at the University of Illinois at Chicago, USA. Single aliquot regeneration (SAR) protocols (Murray and Wintle, 2003) were used in this study to estimate the apparent equivalent dose of the 100–150 or 63–100 μm quartz fraction for up to 60 separate aliquots. Each aliquot contained ~50 to 100 quartz grains corresponding to a 1 mm diameter plate on a circular aluminum disc. The quartz fractions were isolated by density separation using the heavy liquid Na-polytungstate, and a 40-min immersion in HF (40%) was applied to etch the outer ~10 μm of grains, which is affected by α radiation (Mejdahl and Christiansen, 1994). Quartz grains were rinsed finally in HCl (10%) to remove any insoluble fluorides. The purity of quartz separate was evaluated by petrographic inspection and point counting of a representative aliquot.

An automated Risø TL/OSL-DA-15 system was used for SAR analyses. Blue light excitation (470 ± 20 nm) was from an array of 30 light-emitting diodes that deliver ~15 mW/cm^2 to the sample position at 90% power. A Thorn EMI 9235 QA hotomultiplier tube coupled with three 3-mm-thick Hoya U-340 detection filters, transmitting between 290 and 370 nm, measured photon emissions. Laboratory irradiations used a calibrated 90Sr/90Y β source coupled with the Risø reader. Optical stimulation for all samples was completed at an elevated temperature (125 °C) using a heating rate of 5 °C/s. All SAR emissions were integrated over the first 0.8 s of stimulation out of 40 s of measurement, with background based on emissions for the last 30- to 40-s interval. A series of experiments were performed to evaluate the effect of preheating at 180, 200, 220, 240, and 260 °C on isolating the most robust time-sensitive emissions and minimize thermal transfer of the regenerative signal prior to the application of SAR dating protocols (Murray and Wintle, 2003). These experiments entailed giving a known dose (20 Gy) and evaluating which preheat resulted in recovery of this dose. There was concordance with the known dose (20 Gy) for preheat temperatures above 200 °C with an initial preheat temperature of 220 °C for 10 s in the SAR protocols.

Equivalent dose (D_e) values for quartz separates were determined on 25 to 42 aliquots, and the age model used was dictated by overdispersion values. An overdispersion percentage of a D_e distribution is an estimate of the relative standard deviation from a central D_e value in context of a statistical estimate of errors (Galbraith et al., 1999; Galbraith and Roberts, 2012). Overdispersion values ≤20% are routinely assessed for quartz grains that are well light reset, like aeolian sands (e.g., Olley et al., 2004; Wright et al., 2011; Forman et al., 2014), and this value is considered a threshold metric for calculation of a D_e value using the central age model of Galbraith et al. (1999). Overdispersion values >20% indicate mixing of grains of various ages or partial solar resetting of grains; the minimum age model (Galbraith et al., 1999) or finite mixing model (Galbraith and Green, 1990) may be an appropriate statistical treatment for such data. The statistical analysis by a finite mixing model (Galbraith and Green, 1990) showed that D_e distributions for nine of the eleven quartz extracts are negatively skewed. This might be caused by a short distance of aeolian transport with some grains not fully light reset or syndepositional mixing of sediments associated with weak pedogenesis. In either case, the youngest defined D_e population by the finite mixing model or the minimum age model yields a closer estimate of the depositional age. We present D_e values, other details of the dating, and associated apparent ages for all samples by different age models in Table 1. For all samples, at least 25 aliquots were used for the final (*De*) distribution and age determination (Table 1; Supplementary Fig. 1).

Wind records (data obtained online from the U.S. National Climate Data Centre, http://gis.ncdc.noaa.gov/map/viewer/#app=cdo&cfg=cdo&theme=hourly&layers=1) covering the period from 1973 to 2014 from the four meteorological stations (Linhe, Hailiutu, Dongsheng,

Table 1
Optically stimulated luminescence (OSL) ages on quartz grains from aeolian sands, Kubuqi Desert, China (for locations of the samples see Figs. 2, 7–10)

Sample number	Depth (m)	Lab number	Aliquots[a]	Grain size (μm)	De MAM or (CAM)(Gy)[b]	De FMM (Gy)[c]	OD-(%)[d]	U (ppm)[e]	Th (ppm)[e]	K (%)[e]	Cosmic dose (mGy/y)[f]	Dose rate (mGy/y)[g]	CAM or MAM OSL age (y)	FMM OSL age (y)
KA-1	0.8	UIC3435	34/45	63–100	0.46 ± 0.08	0.57 ± 0.07	82 ± 10	1.4 ± 0.1	5.8 ± 0.1	1.65 ± 0.02	0.24 ± 0.02	2.41 ± 0.12	190 ± 35	235 ± 35
KA-2	1.5	UIC3434	39/45	100–150	2.16 ± 0.40	2.14 ± 0.26	80 ± 9	1.5 ± 0.1	6.6 ± 0.1	1.61 ± 0.02	0.22 ± 0.02	2.36 ± 0.12	910 ± 180	905 ± 125
KA-3	2	UIC3441	36/45	63–100	6.76 ± 0.22	4.77 ± 0.39	42 ± 5	1.6 ± 0.1	7.2 ± 0.1	1.63 ± 0.02	0.21 ± 0.02	2.51 ± 0.13	2965 ± 190	1900 ± 195
KA-4	3.4	UIC3445	35/45	63–100	NC	9.03 ± 0.86	41 ± 5	1.4 ± 0.1	6.0 ± 0.1	1.62 ± 0.02	0.18 ± 0.02	2.34 ± 0.12	NC	3850 ± 440
KA-5	4.3	UIC3444	34/60	100–150	10.15 ± 0.47	13.24 ± 1.52	63 ± 8	1.1 ± 0.1	4.4 ± 0.1	1.75 ± 0.02	0.16 ± 0.02	2.18 ± 0.12	4645 ± 380	6060 ± 810
KB-1	0.5	UIC3448	25/30	63–100	NC	5.14 ± 0.45	89 ± 13	1.3 ± 0.1	5.2 ± 0.1	1.67 ± 0.02	0.24 ± 0.02	2.36 ± 0.12		2175 ± 290
KB-2	0.8	UIC3433	28/30	100–150	(6.67 ± 0.37)	6.62 ± 0.40	22 ± 4	1.5 ± 0.1	6.9 ± 0.1	1.68 ± 0.02	0.23 ± 0.02	2.45 ± 0.13	2725 ± 230	2705 ± 235
KB-3	1.4	UIC3442	42/45	63–100	7.34 ± 0.74	7.24 ± 0.44	60 ± 7	1.5 ± 0.1	6.8 ± 0.1	1.69 ± 0.02	0.22 ± 0.02	2.52 ± 0.13	2910 ± 400	2870 ± 320
KB-4	2.2	UIC3440	38/45	100–150	17.74 ± 1.32		78 ± 9	1.4 ± 0.1	5.9 ± 0.1	1.59 ± 0.02	0.20 ± 0.02	2.25 ± 0.12	7870 ± 745	
KC-1	1.2	UIC3436	31/45	63–100	8.00 ± 0.36	8.94 ± 0.57	35 ± 5	1.4 ± 0.1	5.6 ± 0.1	1.57 ± 0.02	0.22 ± 0.02	2.31 ± 0.12	3475 ± 380	3875 ± 460
KC-3	3.6	UIC3449	30/30	63–100	(16.98 ± 0.74)	17.02 ± 0.83	14 ± 2	1.3 ± 0.1	5.6 ± 0.1	1.59 ± 0.02	0.17 ± 0.02	2.26 ± 0.12	7515 ± 580	7520 ± 590
KD-1	0.5	UIC3437	32/60	63–100	32.68 ± 1.16	33.83 ± 1.85	59 ± 7	1.3 ± 0.1	5.3 ± 0.1	1.58 ± 0.02	0.01 ± 0.001	2.08 ± 0.11	15,685 ± 1190	16,240 ± 1410

[a] Aliquots used in equivalent dose calculations versus original aliquots measured.
[b] Equivalent dose (De) calculated on a pure quartz fraction for designated grain size (~2 mm plate area) and analyzed under blue-light excitation. (470 ± 20 nm) by single aliquot regeneration protocols (Murray and Wintle, 2003). Equivalent dose calculated using the minimum (MAM) or central (CAM) age model (Galbraith and Roberts, 2012) based on overdispersion values (at 2 sigma errors) of <20% or >20%, respectively.
[c] Equivalent dose (De) calculated by finite mixer model (FMM) (Galbraith and Green, 1990).
[d] OD = overdispersion values and reflects precision beyond instrumental errors; values of ≤20% (at 2 sigma limits) indicate low dispersion in equivalent dose values and an unimodal distribution.
[e] U, Th and K content analyzed by inductively-coupled plasma-mass spectrometry analyzed by Activation Laboratory LTD, Ontario, Canada.
[f] Cosmic dose rate calculated from parameters in Prescott and Hutton (1994).
[g] A moisture content of 10 ± 3% was assumed for all samples.
[g] Systematic and random errors calculated in a quadrature. Reported errors are at one sigma and reference year for ages is A.D. 2010.

and Huhehaote) in the study area were used to interpret the potential movement of sand. Sand drift potential (DP), resultant drift potential (RDP), the directional variability (RDP/DP which gives a measure of variability in wind direction), and the resultant direction of sand movement (RDD) were calculated (Fig. 1) following Fryberger and Dean (1979). Wind speeds in m/s are used in calculations, and the resultant values are finally converted to vector units with the wind speed in knots (Fryberger and Dean, 1979; Bullard, 1997).

4. Results

4.1. Geomorphology of the Kubuqi sand sea

Aeolian sands of the Kubuqi Desert are mostly confined to the hilly landscape of the northern slope facing the Yellow River. Sand ramps emanating from the Yellow River are common with superimposed barchanoid dune forms. These aeolian sands can be traced up tributary valleys orientated north to south and appear to bury the risers and treads of fluvial terraces. Large dunes are absent in western part of the Kubuqi Desert (Figs. 1 and 2). Instead this area is covered by sand sheet deposits and small barchanoid dunes. Some transverse dunes in the Kubuqi sand sea appear to be 100 m high from the lowest elevations to ridge tops. However, this topography may reflect a palimpsest landscape with a sand sheet deposit burying river terraces. The aeolian sands in the Kubuqi Desert also in places cover bedrock surfaces and may be recent deposits. For example, section [*a*] consists of thin aeolian sands over mudstones and is located on the east side of the dune resort named Xiangshawan (meaning bay of singing sands) where hotels were built on higher parts of the bedrock hills (Fig. 3).

The grain size data of samples from the dune ridges indicate that the dune sands in the Kubuqi are composed principally of medium to fine sands (Fig. 4). The mean grain size varies between 90 and 180 μm, and the largest size fraction is 125–250 μm in the active and vegetation-stabilized dune ridges sand, except for samples 6 and 11 (Figs. 4 and 5), in which the finer fraction (<125 μm) accounts for nearly 50%. The sand samples from an east–west transection across the dune field are very well sorted to well sorted (Folk and Ward, 1957) with σ values between 0.2 and 0.5. The frequency distribution of grain sizes is positively skewed (*Sk*) with a tail of finer grains. The kurtosis values (*Kg*) vary between 1.0 and 1.15, suggesting that the distribution curve of grain size frequencies is mainly mesokurtic (Fig. 4). The grain size distribution curves of samples from the Kubuqi sand sea show a similar unimodal distribution, with a main mode at 2.7–3φ (150–125 μm). Only one sample (sample 11) is, however, characterized by a slightly

Fig. 3. Dune landscape of the Kubuqi, viewing from the valley side of section [*a*] toward the west. The valley in the middle is a tributary channel of the Yellow River. The white building (resort hotels) and vegetation in the distance mark the occurrence of mudstone bedrock on the surface.

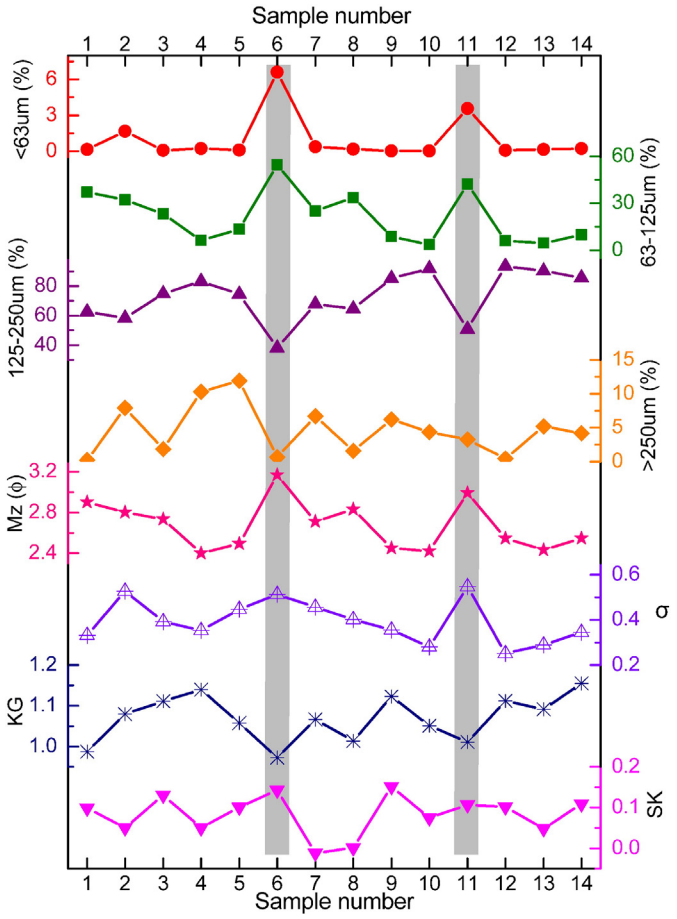

Fig. 4. Compositions (upper) and grain size parameters (lower) of surface sand samples taken from the Kubuqi (for sampling sites see Fig. 2).

bimodal distribution, with a secondary peak at around 3.73φ (75 μm; Fig. 5).

4.2. Potential sand transport

Wind roses based on monthly records from 1973 to 2014 in the margins of the desert display a distribution pattern dominated by northwest and west winds (Fig. 1), but a generally low drift potential value from the northwest between 84 and 318 VU (Fig. 1) suggests that the sand sea is in a low-energy wind environment. Whereas higher drift potentials are calculated for the northwest side of the desert (Fig. 1), implying that wind is efficient to transport sand from the Yellow River valley to the desert, but further transport of sand is minor once in the area. The monthly total DP and sand roses of the Dongsheng weather station represent a great seasonal variation (Fig. 6). Spring and winter are seasons of the greatest sand transport activity, contributing to about 70% of annual sand transport. The lowest DP value is reached in summer (July, August, and September). The monthly sand roses show that our study area is dominated by a strong northwesterly wind in late winter and early spring and a gentle southeasterly wind in summer.

4.3. Aeolian sedimentology and associated OSL ages

Four stratigraphic sections with multiple aeolian sand units and palaeosols have been carefully investigated. Section [*a*] (109°57′, 40°14′; Fig. 7; Table 1) is exposed at 100 m above a tributary channel of the Yellow River, and it was cut by the fluvial incision of the tributary. It is composed of ~4.4 m of aolian fine sand with depositional units differentiated by one palaeosol. The lowest unit 1 (4.4–4 m) is light yellowish brown (10YR 6/4), moderately sorted, aeolian fine sand, with quartz grains from the base of this unit yielding an OSL age of 6060 ± 810 y. The upper 60 cm of unit 1 is yellowish brown (10YR 6/6), moderately well sorted, fine to medium aeolian sand. Unit 2 (3.4–1.4 m) is a palaeosol layer, with a brown (10YR 5/3), poorly sorted, silty fine sand. The sand of unit 2 is chronologically constrained by three OSL ages yielding, at the base, 3850 ± 440 y and 1900 ± 195 y above. The cultural layer of the upper 10 cm of unit 2 is moderately sorted, silty sand, contains some carbon bits, and is OSL dated to 905 ± 125 y. Unit 3 (1.4–0 m) is characterized by light yellowish brown (10YR 6/4), moderately well sorted, fine sand. Quartz grains from the middle of this unit returned an OSL age of 235 ± 35 y.

Section [*b*] (109°47′, 40°16′; Fig. 8) is located in the terrace ca. 20 m above the current river bed of the tributary with headwaters in the southern Erdos Plateau. The terrace riser is just visible beneath aeolian sands and is covered by a 20-*m*-high transverse dune. Two distinct aeolian depositional units are separated by a buried palaeosol in this section. The basal unit 1 (3.2–2.4 m) is light yellowish brown (10YR 6/4), moderately well sorted, fine sand. The OSL sample at 2.9 m yielded an age of 7870 ± 745 y. The palaeosol layer of unit 2 (2.4–0.35 m) is dark grayish brown (10YR 4/2), poorly sorted, silty sand; while the top 40 cm of this unit is differentiated by a more weak buried soil with a weak blocky structure, brown (10YR 5/3), moderately sorted, silty sand and pedogenic, small carbonate pebbles. The palaeosol in this section appears to be cummulic A horizons, with bracketing OSL ages indicating that ensuing pedogenesis occurred between 2870 ± 320 y and

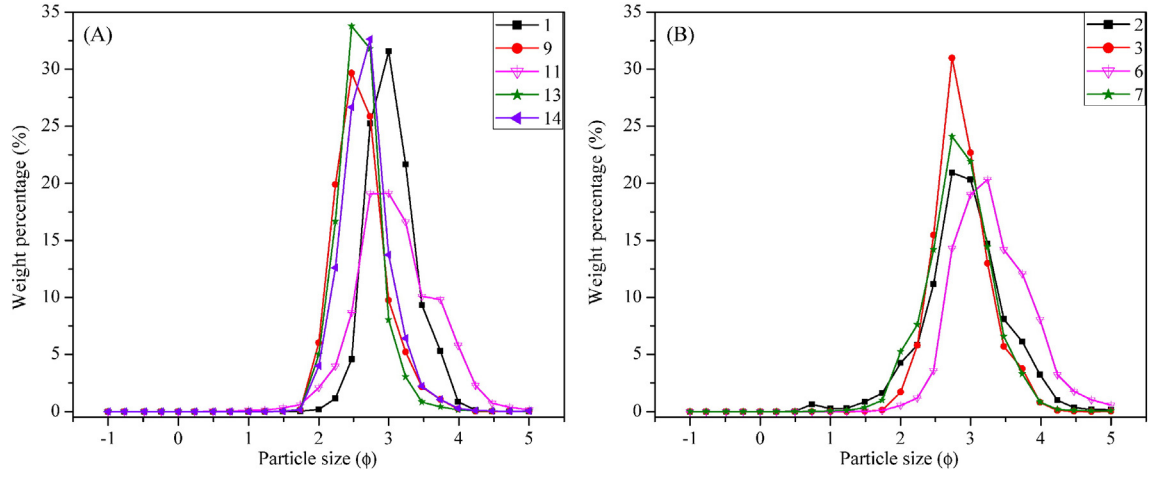

Fig. 5. Grain size distribution of dune sands in the Kubuqi sand sea. (A) and (B) refer to samples from active and vegetable-stabilized dunes' ridges, respectively.

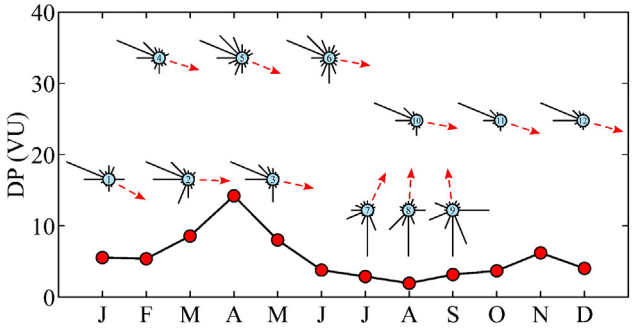

Fig. 6. Monthly values of DP and sand roses in Dongsheng (for location see Fig. 1). Number refers to the relevant month, respectively.

2175 ± 290 y. This buried soil has been truncated by emplacement of unit 3 (0.35–0 m), light yellowish brown (10YR 6/4), very well sorted, medium sand.

Section [*c*] (108°56′, 40°22′; Fig. 9) is located on the top of the first terrace of the stream Maobulakongdui, and this site is 22 m above the current river bed. It consists of aeolian sands in the bottom and intercalations between flood deposits and aeolian sands in the upper part. The base part (3.7–0.7 m) is characterized by light yellowish brown (10YR 6/4), well sorted, fine sand. Flood deposits in the upper part (0.7–0 m) are light brown (7.5YR 6/3), poorly sorted, clayey silt with Machete's (1985) stage 2 carbonate filaments and strong blocky structure. Two very hard calcareous cementation layers are identified with a thickness of ~2 cm, white (5YR 8/1), silty sands. This section represents the latest stage of a flooding when the river bed was at that height. The OSL ages indicate that the river bed elevation was quasi-stable between 7520 ± 590 and 3875 ± 460 y, and aeolian sedimentation occurred probably near the river course. An OSL age on the overlying aeolian sand indicates that fluvial incision occurred after 3875 ± 460 y (Fig. 9).

The oldest aeolian deposit identified is exposed as a subhorizontal-bedded, white (5YR 8/1), poorly sorted, medium sand in section [*d*] (108°59′, 40°24′; Fig. 10) and contains some subrounded gravels with a diameter of 2–3 mm, from which quartz grains yielded an OSL age of 16,240 ± 1410 y. The section is exposed at a low elevation close to the main channel of the Yellow River, and it was cut by the fluvial incision of a tributary. We think that the site was originally part of the river channel (Fig. 1) and that the sands had been accumulated as deposits of the flooding plain of the river system at earlier stages.

The bases of three of the four sections appear to be Holocene age, while the section with older aeolian sands (Fig. 10) is located on the bank of the river. The palaeoenvironmental proxies like mean grain size, sorting (σ), content of calcium carbonate, magnetic susceptibility, and content of total carbon and total organic carbon vary between aeolian sands and layers of palaeosols (Figs. 7–9). Apparently, the sediments of aeolian sands are coarser and better sorted than those of palaeosols. Calcium carbonate, total carbon, and total organic carbon contents are generally higher in the palaeosols than in the aeolian sands. The percentage frequency dependent magnetic susceptibility (χ_{fd}) is clearly higher in palaeosols than in the aeolian sands, although the magnetic susceptibility of low field (χ_{lf}) does not present a clear difference between aeolian sands and palaeosols (Figs. 7–9).

5. Discussion

The grain size parameters for sediments taken from the Kubuqi Desert do not exhibit any distinctive spatial trend. We identify no trend in grain size variations over the 260-km-long distance from west to east nor significant variations along the tributaries crossing the desert belt from south to north (between samples 1 and 14; Figs. 2 and 4). For example, samples 6 and 11 are characterized by a higher percentage of silt and smaller mean grain size, but one from the western part and the other from the eastern end show no trends of fining along the predominant wind directions (Figs. 2 and 4). The heterogeneity of grain size distribution possibly indicates that sands of the Kubuqi Desert were not sourced from a single site. Thus the occurrence of the aeolian deposits along the southern margin of the Yellow River, i.e., the Kubuqi, is probably related to the availability of sediments in this wide valley reflecting a variable flood regime and persistent winds from the north and west (Figs. 1 and 6). A similar phenomenon should also have occurred in the Maowusu Sandy Land (which is located south of the Kubuqi), whose sand materials were brought from the Yellow River by fluvial-aeolian processes (Stevens et al., 2013). The positive skewness of all samples (high percentage of fine grains) may be indicative of active aeolian processes and *young* ages of the aeolian sediments (Besler, 1980), though the particle size characteristics are consistent with sand sheet deposits (Forman et al., 2014). The occurrence of threshold wind speeds

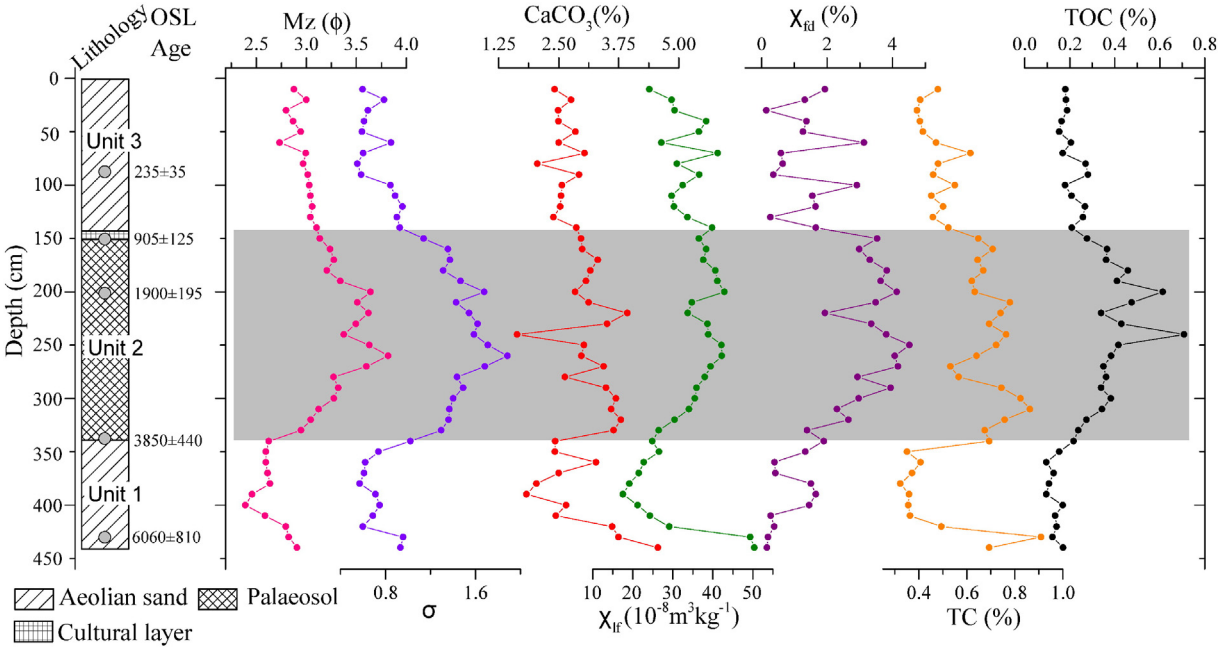

Fig. 7. The stratigraphy, OSL chronology, and changes of palaeoenvironmental proxies in section [*a*].

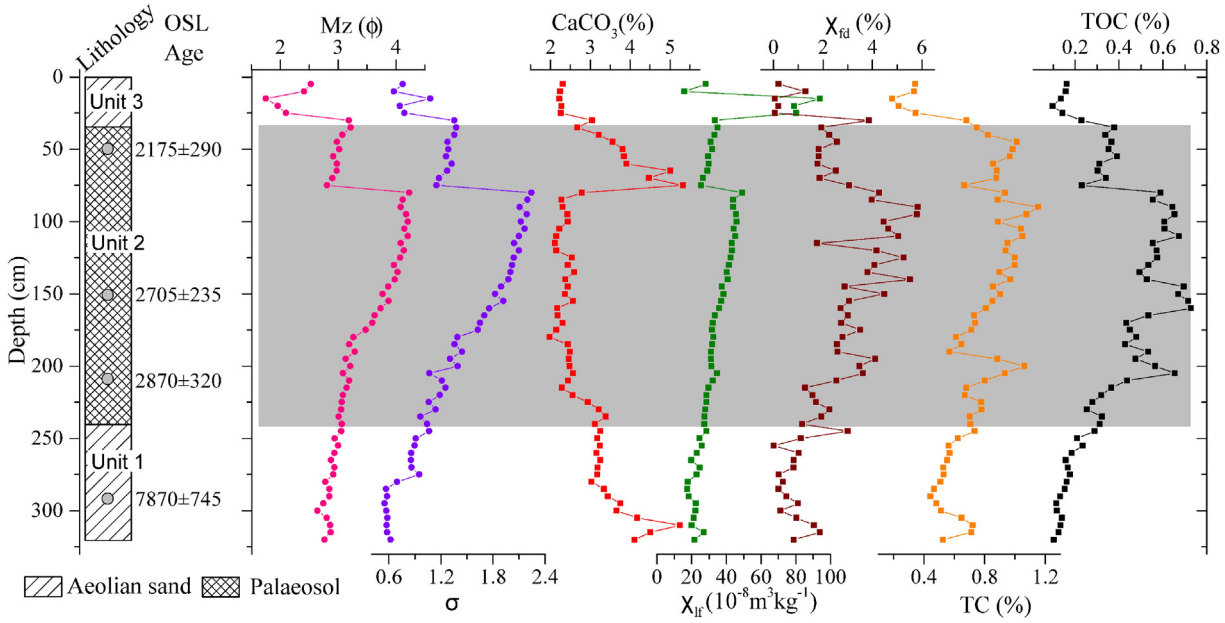

Fig. 8. The stratigraphy, OSL chronology, and changes of palaeoenvironmental proxies in section [*b*].

(>5 m/s) from many directions in the region theoretically should yield a variety of dune types in the Kubuqi Desert, but often just sand ramps occur instead of dunes.

Exposures in the Kubuqi sand sea provide new insights on the sedimentologic record of aeolian deposition and associated age. However, the four presented sections are just limited examples for a better understanding of the complex history of dune movement and stability in the sand sea. The oldest aeolian deposit with the OSL age of 16,240 ± 1410 y, located near the river channel (Fig. 10), should be associated with a source-bordering dune (Williams, 2014a; Al-Masrahy and Mountney, 2015); and its formation should be closely linked to fluvial sediment sources rather than climatic aridity. Thus it could not be a convincing indicator for the occurrence of the desert landscape in the region but reflects an increased sediment availability during this period (Williams, 1994; Maroulis et al., 2007; Cohen et al., 2010; Halfen et al., 2015). As Williams (1994) pointed out, source-bordering dune development in western New South Wales of Australia was enhanced at times of warmer and wetter climate by replenishment of the localized fluvial-sand supply. Fan et al. (2013) presented an 80-cm-thick section from the northwestern part of the Kubuqi Desert with OSL ages of ca. 19 ka at a depth of 70 cm and ca. 14 ka at a depth of 40 cm. Although Fan et al. (2013) reported that these ages should reflect the initial ages of the Kubuqi Desert, we think that the sediments of this section would be associated with shoreline deposits rather than sediments of sand seas because of its location in a former lake environment. We note that all OSL samples reported in Fan et al. (2013) were taken

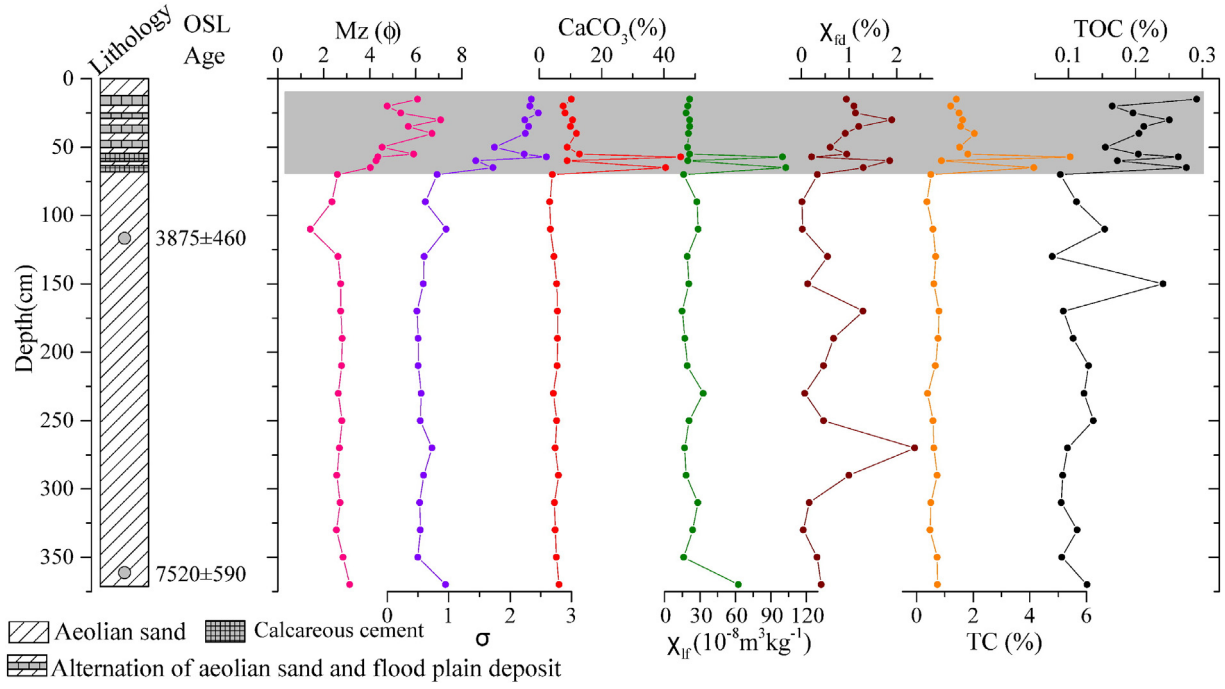

Fig. 9. The stratigraphy, OSL chronology, and changes of palaeoenvironmental proxies in section [*c*].

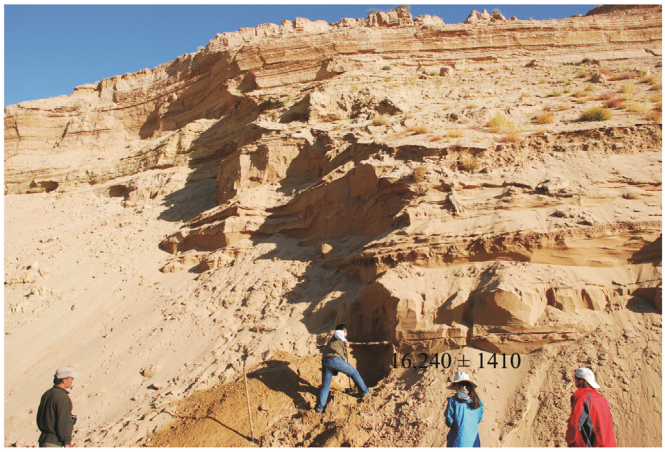

Fig. 10. Photo of section [*d*] and the OSL chronology (sample taken from the hole we just dug) from the base of the section. The hard thin layers are calcareous cementations occurring from the bottom to the top.

from the upper 1 m and all others were dated to Holocene age, broadly consistent with our interpretation that the age of modern desert landscape formation could not predate the Holocene.

Our sections [*a*], [*b*], and [*c*] all overlie bedrock or fluvial terraces, and their OSL chronologies show that the ca. 4-m aeolian sands as landscape palimpsest have been deposited sometime in the last ca. 8 ka. We identified two buried soils with cummulic A horizons, reflecting a reduction in sediment deposition for prolonged century- to millennial-scale periods sometime between ca. 4 and 0.9 ka, as Figs. 8 and 9 show. The organic carbon (TOC) content of aeolian sequences is related to onsite vegetation types; and in general, the palaeosols correspond to grass-steppe or forest-steppe, and dune sands correspond to desert landscape in central Inner Mongolia (Sun et al., 2006). In our sections (Figs. 7 and 8), high TOC contents occurred in the buried soils, whereas low TOC occurred in the aeolian sand beds. This, together with the changes of magnetic susceptibility, indicates that the period from ~4 to ~2 ka was probably an episode of increased precipitation or effective moisture that was advantageous to vegetation growth, soil development and organic matter accumulation. Our palaeoenvironmental interpretation of the sand–palaeosol sequences in the Kubuqi is broadly consistent with the palaeoclimatic reconstructions based on the lacustrine records not far from the south (Sun and Feng, 2013). Based on the fossil pollen record in the Qigai Nuur (lake) in the northern Maowusu Desert, Sun and Feng (2013) suggested that the landscape was probably a steppe under cool conditions at the interval of ~4000 to ~2800 cal. y BP.

Burial of the palaeosols in the Kubuqi, as shown in Figs. 7 and 8, by aeolian sand appears to have been intensified 2000 and 1000 years ago by human expansion into this area during the Han (202 B.C.–A.D. 220) and Tang (A.D. 618–907) dynasties. Detailed study of these buried soils is warranted to better understand palaeoenvironments. We are not yet sure whether the aeolian sand depositional events within the Holocene reflect additional source material from the Yellow River and/or multiple sources from previously deposited aeolian sand, particularly within the interior of the dune field.

A critical aspect of assessing the processes and causes of aeolian activity in the Kubuqi sand sea is a better understanding of human disturbance in this *sandy land* in the late Holocene. Obviously, grazing and agricultural activity can lead to landscape degradation and aeolian reactivation in mesic and semiarid environments (e.g., Zhu et al., 1980; Forman et al., 2008a, 2008b; Tripaldi et al., 2013). Various historical records demonstrate that a number of county-level cities or population centers occurred in the Kubuqi sand sea (Wang, 1991). Settlements during the Han (202 B.C. – A.D. 220) and Tang (A.D. 618–907) dynasties occurred in the Kubuqi Desert, although cities may have existed as early as ca. 3000 years ago (Wang, 1991). Two historical books reported that the military of the Han Dynasty occupied the areas south of the Yellow River in 127 B.C. and the district administration center of Sufangjun was established and governed 10 counties (Ban Gu, 206 B.C.–A.D. 220 ; Li Daoyuan, A.D. 439–534). This center, which is now the Kubuqi Desert, was developed to spur the regional economy at the northwestern boundary of the Chinese nation at that time. Sufangjun city had over 20,000 residents in the western Kubuqi Desert in the period from the Han Dynasty (202 B.C.–A.D. 220) to the Tang Dynasty (A.D. 618–907) (Wang, 1991).

Wang (1991), from historical accounts, located the site of the Guangmu County seat of the Han Dynasty, which currently is covered by aeolian sands. However, no archaeological excavation to search for the remains of this city has been carried out. According to the historical descriptions, the site of the Han's Guangmu County was the same place of the Fengzhou City of the Tang Dynasty (Wang, 1991), roughly 50 km southwest of our sampling site 13 (Fig. 2). During our field work, we often saw artifacts like ceramics in the dune fields, confirming human activities in earlier times. Historical records indicate that Guangmu was a large county during the Han Dynasty, and 3000 families subsisted by agriculture in the county (Wang, 1991). During the Han Dynasty, a county named Huzun existed in the middle reaches of the tributary Maobulakundui (Wang, 1991), i.e., near our sections [*c*] and [*d*] (Fig. 2), but the area is now buried under aeolian sands (Fig. 11). Descriptions about occurrence of aeolian sands in the region appeared during the Tang Dynasty for the first time, but a large oasis occurred between the Yellow River and Fengzhou City during the Tang Dynasty (Wang, 1991). A historical analysis of prehistoric population inferred from the book 'New Tang Notes, Volume Geography' (Ouyang Xiu and Song Qi, A.D.618–907) shows a population of 9641 people (with 2813 families), which included Chinese families but not the other minorities in the territories of Fengzhou. Thus the population may have been greater than the historical analysis (Wang, 1991).

Because cities were built in the Kubuqi as early as ca. 3000 years ago (Wang, 1991), people in these cities must be dependent on water from the Yellow River at that time already. Diversion of water could cause desiccation of some parts of river beds, as the common cases nowadays in western China (Yang et al., 2006). The area increase of dried fluvial beds by the initiation of irrigation ca. 3 ka ago probably provided an additional source area for aeolian sands within the valley. Thus human water use in the upper drainages of the Yellow River during historical times may have contributed to the formation of this sand sea. In particular, the expansion of cities and agricultural activities during the Han and Tang dynasties within the Kubuqi Desert may have resulted in broad-scale land degradation. Animal grazing and farming around these ancient cities may have been detrimental to the quasi-stable vegetated surface, as identified as palaeosols in the stratigraphic assessments. Thus we hypothesize that renewed aeolian activity from human-induced landscape degradation may have been pivotal in forming this enigmatic, inland sand sea in the late Holocene.

6. Conclusions

The Kubuqi Desert, an active sand sea in semiarid northern China has a distinct history and processes dissimilar to the more arid deserts in northwestern China. These aeolian deposits occur mainly on the north slope of the Erdos Plateau's southern margins. Many of the dunes in the Kubuqi sand sea cover bedrock and are palimpsest with underlying fluvial terraces. Reconnaissance aeolian stratigraphic assessment coupled with OSL dating indicate that the sediments near river channels or lake basins should not be seen as evidence of the occurrence of the sand seas because of their direct association with local fluvial or lacustrine processes. The upper 2–4 m of sands, forming the palimpsest of the landscape and OSL dated to the Holocene, are representative of the large-scale occurrence of aeolian processes and the initial formation of the Kubuqi sand sea. The latest period of aeolian deposition overlying a prominent buried soil ca. 1000 to 2000 years ago may be related to

Fig. 11. Dramatic changes of the landscape in the Kubuqi. Left: Dune landscape occurring in areas of the Hunzun County site during the Han Dynasty. Right: Artifacts (ceramics) occurring on the dunes nearby.

human activity associated with grazing and farming from *lost* cities of the Han (206 B.C.–A.D. 220) and Tang (A.D. 618–907) dynasties that once occurred in the Kubuqi. In turn, variable discharge of the Yellow River with diversions for irrigation may have resulted in a more consistent supply of aeolian particles for dune field expansion. The current active sand sea may be a legacy of landscape degradation during the Han and Tang dynasties and broader human disturbance within the Yellow River catchment.

Supplementary data to this article can be found online at http://dx.doi.org/10.1016/j.geomorph.2016.02.004.

Acknowledgements

This collaborative research was supported by the CAS Strategic Priority Research Program (grant no. XDA05120502) and the National Natural Science Foundation of China (Grant no. 41430532). We also acknowledge the help from Qianqian Liu, Xiaozun Ren, and Annette Süssenberger during the field work. Sincere thanks are extended to Editor Prof. Richard A. Marston and two anonymous reviewers for their constructive comments on the earlier draft of this paper. Prof. Richard A. Marston has also graciously edited the entire manuscript.

References

Al-Masrahy, M.A., Mountney, N.P., 2015. A classification scheme for fluvial–aeolian system interaction in desert-margin settings. Aeolian Res. 17, 67–88.
Ban Gu, 206B.C.–A.D. 220 (Han Dynasty). Han Notes, Volume Geography. China (in classic Chinese).
Besler, H., 1980. Die Duenen-Namib: Entstehung und Dynamik eines Ergs. Stuttgarter Geographischen Studien 96, 1–241.
Bullard, J., 1997. A note on the use of the "Fryberger method" for evaluating potential sand transport by wind. J. Sediment. Res. 67, 499–501.
Busche, D., 1998. Die Zentrale Sahara. Justus Perthes, Gotha.
Chase, B., 2009. Evaluating the use of dune sediments as a proxy for palaeo-aridity: a southern African case study. Earth Sci. Rev. 93, 31–45.
Cohen, T.J., Nanson, G.C., Larsen, J.R., Jones, B.G., Price, D.M., Coleman, M., Pietsch, T.J., 2010. Late Quaternary aeolian and fluvial interactions on the Cooper Creek Fan and the association between linear and source-bordering dunes, Strzelecki Desert, Australia. Quat. Sci. Rev. 29, 455–471.
Dearing, J.A., 1999. Environmental Magnetic Susceptibility: Using the Bartington MS2 System. Bartington Instruments Limited, Oxford.
Domrös, M., Peng, G., 1988. The Climate of China. Springer-Verlag, Berlin Heidelberg New York.
Eitel, B., Hecht, S., Mächtle, B., Schukraft, G., Kadereit, A., Wagner, G., Kromer, B., Unkel, I., Reindel, M., 2005. Geoarchaeological evidence from desert Loess in the Nazca-Palpa Region, Southern Peru: Palaeoenvironmental changes and their impact on pre-Columbian cultures. Archaeometry 47, 137–158.
Embabi, N.S., 2004. The Geomorphology of Egypt: Landforms and Evolution, Volume I The Nile Valley and the Western Desert. The Egyptian Geographical Society, Cairo.
Fan, Y., Chen, X., Fan, T., Jin, M., Liu, J., Chen, F., 2013. Sedimentary and OSL dating evidence for the development of the present Hobq desert landscape, northern China. Science China. Earth Sciences http://dx.doi.org/10.1007/s11430-013-4673-7 (in Chinese).
Folk, R., Ward, W., 1957. Brazos river bar: a study in the significance of grain size parameters. J. Sediment. Petrol. 27, 3–26.
Forman, S.L., Sagintayev, Z., Sultan, M., Smith, S., Becker, R., Kendall, M., Marin, L., 2008a. The migration of parabolic dunes and wetland formation at Cape Cod National Sea Shore, MA: landscape response to a legacy of environmental disturbance. The Holocene 18, 765–774.
Forman, S.L., Marín, L., Gomez, J., Pierson, J., 2008b. Late Quaternary eolian sand depositional record for southwestern Kansas: landscape sensitivity to droughts. Palaeogeogr. Palaeoclimatol. Palaeoecol. 265, 107–120.
Forman, S.L., Tripaldi, A., Ciccioli, P.L., 2014. Sand sheet deposition in the San Luis paleodune field, western Argentina as an indicator of a semi-arid environment through the Holocene. Palaeogeogr. Palaeoclimatol. Palaeoecol. 411, 122–135.
Fryberger, S.G., Dean, G., 1979. Dunes forms and wind regime. In: McKee, E.D. (Ed.), A Study of Global Sand SeasGeological Survey Professional Paper 1052. U.S. Government Printing Office, Washington, pp. 137–170.
Galbraith, R.F., Green, P.F., 1990. Estimating the component ages in a finite mixture. Nucl. Tracks Radiat. Meas. 17, 197–206.
Galbraith, R.F., Roberts, R.G., 2012. Statistical aspects of equivalent dose and error calculation and display in OSL dating: an overview and some recommendations. Quat. Geochronol. 11, 1–27.
Galbraith, R.F., Roberts, R.G., Laslett, G.M., Yoshida, H., Olley, J.M., 1999. Optical dating of single and multiple grains of quartz from jinmium rock shelter, northern Australia, part 1, experimental design and statistical models. Archaeometry 41, 339–364.
Goudie, A.S., 2002. Great Warm Deserts of the World: Landscapes and Evolution. Oxford University Press, New York.
Halfen, A.F., Lancaster, N., Wolfe, S., 2015. Interpretations and common challenges of aeolian records from North American dune fields. Quaternary International http://dx.doi.org/10.1016/j.quaint.2015.03.003.
Hövermann, J., 1985. Das System der klimatischen Geomorphologie auf landschaftskundlicher Grundlage. Z. Geomorphol. Suppl. 56, 143–153.
Kocurek, G., Lancaster, N., 1999. Aeolian system sediment state: theory and Mojave Desert Kelso dune field example. Sedimentology 46, 505–515.
Lancaster, N., 1995. Geomorphology of Desert Dunes. Routledge, London.
Li Daoyuan, A.D. 439–534 (Northern Wei Dynasty). Hydrological Notes. China (in classic Chinese).
Liu, T., 1985. Loess and the Environment. China Ocean Press, Beijing.
Ma, L. (Ed.), 2002. Geological Atlas of China. Geological Press, Beijing (in Chinese).
Machette, M., 1985. Calcic soils of southwestern United States. In: Weide, D.J. (Ed.), Soil and Quaternary Geology of the Southwestern United States. Geological Society of America, Special Paper 203, pp. 1–21.
Maroulis, J.C., Nanson, G.C., Price, D.M., Pietsch, T., 2007. Aeolian-fluvial interaction and climate change: source-bordering dune development over the past ~100 ka on Cooper Creek, central Australia. Quat. Sci. Rev. 26, 386–404.
Mejdahl, V., Christiansen, H.H., 1994. Procedures used for luminescence dating of sediments. Boreas 13, 403–406.
Muhs, D.R., Holliday, V.T., 1995. Evidence of active dune sand on the Great Plains in the 19th century from accounts of early explorers. Quat. Res. 43, 198–208.
Murray, A.S., Wintle, A.G., 2003. The single aliquot regenerative dose protocol: potential for improvements in reliability. Radiat. Meas. 37, 377–381.
Olley, J.M., Pietsch, T., Roberts, R.G., 2004. Optical dating of Holocene sediments from a variety of geomorphic settings using single grains of quartz. Geomorphology 60, 337–358.
Prescott, J.R., Hutton, J.T., 1994. Cosmic ray contributions to dose rates for luminescence and ESR dating: large depth and long time variations. Radiat. Meas. 23, 497–500.
Stevens, T., Carter, A., Watson, T.P., Vermeesch, P., Andò, S., Bird, A.F., Lu, H., Garzanti, E., Cottam, M.A., Sevastjanova, I., 2013. Genetic linkage between the Yellow River, the Mu Us desert and the Chinese Loess Plateau. Quat. Sci. Rev. 78, 355–368.
Sun, A., Feng, Z., 2013. Holocene climatic reconstructions from the fossil pollen record at Qigai Nuur in the southern Mongolian Plateau. The Holocene 23, 1391–1402.
Sun, J., Li, S., Han, P., Chen, Y., 2006. Holocene environmental changes in the central Inner Mongolia, based on single-aliquot-quartz optical dating and multi-proxy study of dune sands. Palaeogeogr. Palaeoclimatol. Palaeoecol. 233, 51–62.
Telfer, M., Hesse, P., 2013. Palaeoenvironmental reconstructions from linear dunefields: recent progress, current challenges and future directions. Quat. Sci. Rev. 78, 1–21.
Thomas, D., 2011. Reconstructing paleoenvironments and palaeoclimates in drylands: what can landform analysis contribute? Earth Surf. Process. Landf. http://dx.doi.org/10.1002/esp.3190.
Tooth, S., 2008. Arid geomorphology: recent progress from an Earth System Science perspective. Prog. Phys. Geogr. 32, 81–101.

Tripaldi, A., Zárate, M.A., Forman, S.L., Badger, T., Doyle, M.E., 2013. Drought episode in the western Pampas (Argentina, South America) during the early-mid 20th century: geological evidence, climatic pattern and paleoclimatic inferences. The Holocene 23, 1729–1744.
Wang, B., 1991. Historical geography study of the Kubuqi Desert. Journal of Desert Research 11 (4), 33–41 (in Chinese).
Williams, M., 1994. Some implications of past climatic changes in Australia. Trans. R. Soc. S. Aust. 118, 17–25.
Williams, M., 2014a. Interactions between fluvial and eolian geomorphic systems and processes: examples from the Sahara and Australia. Catena 134, 4–13.
Williams, M., 2014b. Climate Change in Deserts: Past, Present and Future. Cambridge University Press, New York.
Williams, M., Dunkerley, D., De Deckker, P., Kershaw, P., Chappell, J., 1998. Quaternary Environments. second ed. Arnold, London.
Wright, D.K., Forman, S.L., Waters, M.R., Ravesloot, J.C., 2011. Holocene eolian activation as a proxy for broad-scale landscape change on the Gila River Indian Community, Arizona. Quat. Res. 76, 10–21.
Ouyang Xiu, Song Qi, A.D. 618–907 (Tang Dynasty). New Tang Notes Volume Geography. China (in classical Chinese).
Yang, X., Scuderi, L.A., 2010. Hydrological and climatic changes in deserts of China since the late Pleistocene. Quat. Res. 73, 1–9.
Yang, X., Dong, J., White, P., 2006. The key role of water resources management in ecological restoration in western China. Geographical Research (Journal of the Institute of Australian Geographers) 44, 146–154.
Yang, X., Scuderi, L., Paillou, P., Liu, Z., Li, H., Ren, X., 2011. Quaternary environmental changes in the drylands of China - A critical review. Quat. Sci. Rev. 30, 3219–3233.
Yang, X., Li, H., Conacher, A., 2012. Large-scale controls on the development of sand seas in northern China. Quat. Int. 250, 74–83.
Yang, X., Wang, X., Liu, Z., Li, H., Ren, X., Zhang, D., Ma, Z., Rioual, P., Jin, X., Scuderi, L., 2013. Initiation and variation of the dune fields in semi-arid northern China - with a special reference to the Hunshandake Sandy Land, Inner Mongolia. Quat. Sci. Rev. 78, 369–380.
Zhu, Z., Wu, Z., Liu, S., Di, X., 1980. An Outline of Chinese Deserts. Science Press, Beijing (in Chinese).